A Phase-Control Approach for a Large-Element Coherent Microwave Power Uplink System

Richard M. Dickinson, *Life Senior Member, IEEE*, David L. Losh, Robert Dan Barber, and John K. Dempsey

***Abstract*— Signal combining efficiencies of 98% have been achieved on low-earth orbiting (LEO) debris with phase-locking of time-overlapped radar pulses from a two-element phased-array consisting of two 34-m beam waveguide steerable paraboloid antennas separated by 204 m. The uplink arraying at 7.19 GHz has been achieved for tracks from about 10° elevation at signal rise to 4° elevation at signal set under varying weather conditions (e.g., hail falling on one antenna). The typical root mean square (rms) phase error for two coherent 100-μs 50-Hz 5-kW peak pulses reflected from LEO debris with signal-to-noise ratio (SNR) $>$ 23 dB is less than 4°. The phase-control system design, methods of calibration, and details of the design control table of phasing error contributors are presented and discussed. Based upon the measured performance, we predict that transmitting antennas for the Deep Space Network (DSN) could be coherently arrayed for up to hours at a time given static phase error calibrations on exo-atmospheric debris. Applications for this technique include low-cost implementation of high-power microwave transmitters for deep-space communication and radars for exploration of other planets and as part of a defense against comets and asteroids.**

***Index Terms*—Antenna arrays, phased arrays.**

I. Introduction

COHERENT uplink arraying of signals to space objects in real time from widely spaced array elements on earth has been very difficult if not impossible. Because the phase path length is unknown *a priori*, one is just as likely to produce a null on the target as the desired signal peak. In addition to the geometrical difference in path length, there exists uncertainty due to equipment delay variations that are unique to each transmitter–antenna element pair. These equipment variations are due to supply voltages, temperature, gravity loading, and structural wind deflections, for example. The other principal factors are effects such as the variable distribution of water vapor in the earth's atmosphere [1]–[3]. These turbulent structures, modeled as blobs of fluctuations in refractive index and humidity gradients, produce phase variations and scintillations across the transmitting array aperture [4]–[7].

Downlink arraying of signals from space has been successfully accomplished in radio astronomy and deep-space communication since the early days of the space program [8]. Notable recent applications include the arraying of the 27-element 25-m very large array (VLA) antennas and the 70- and 34-m antennas of the Deep Space Network (DSN) at X band for planetary radar returns from Triton and the Voyager data return from Neptune. Also, the Canberra 70-m and the Japanese 64-m antenna at Usuda for voyager radio science enhancement.

The very long baseline interferometer (VLBI) arrays are continents apart and the phase differences can be adjusted in the data after it is received to yield the required coherent summation of contributions from different elements. Instrumentation and propagation delays are adjusted *a posteriori* by signal processing using recorded data. For uplink arraying, that option is not available because the propagation paths change unpredictably and must be accommodated in real time.

This paper describes an approach to uplink arraying using a radar array and demonstrated for the U.S. Army MICOM in 1993 using a pair of 34-m-diameter steerable parabolic reflector antennas equipped with low-power pulsed X-band transmitters (see Fig. 1). The transmitting elements were fed from a common oscillator source. A common receiver was used to measure in real time the phase-path differences from individual transmitters via signals scattered from orbiting debris. The measured results were used to derive the propagation and equipment phase-path length differences. Conjugate phases incorporating the predicted geometry path lengths were then applied through a phase-locked loop for the uplink signals. They array was thus retrodirectively phased on the exo-atmospheric target. The system capabilities have been presented previously [9].

Coherent uplink arraying allows one to achieve a high-power microwave beam using several existing relatively low-cost sources while also providing system benefits in terms of increased availability, incremental growth capability, overall operations and maintenance cost savings, and economies in procurement by taking advantage of quantity purchase discounts.

Power on a target is the square of the electric field vector divided by impedance ($P = E^2/Z$, where Z is the impedance of free-space in this case). Perfectly coherent (in-phase) combining of multiple beams causes the power to increase as the square of the sum of the individual electric fields. Thus, assuming that the power output of each of N sources is P, the power at the target is the same as if the source had a power output of $\eta N^2 P$, where η is the combining efficiency of the system and is comprised of spatial, temporal, polarization, availability, and phase coherence factors of which phase coherence is generally the most difficult to achieve at microwave frequencies. Applications for this technique include radar astronomy and high-power radar applications needed to support a planetary defense system for comets and asteroids [10].

Manuscript received May 29, 1997. This work was supported by the Jet Propulsion Laboratory, California Institute of Technology under contract to the National Aeronautics and Space Administration by the U.S. Army.

The authors are with Jet Propulsion Laboratory, Pasadena, CA 91109 USA.

Publisher Item Identifier S 0018-926X(99)04426-9.

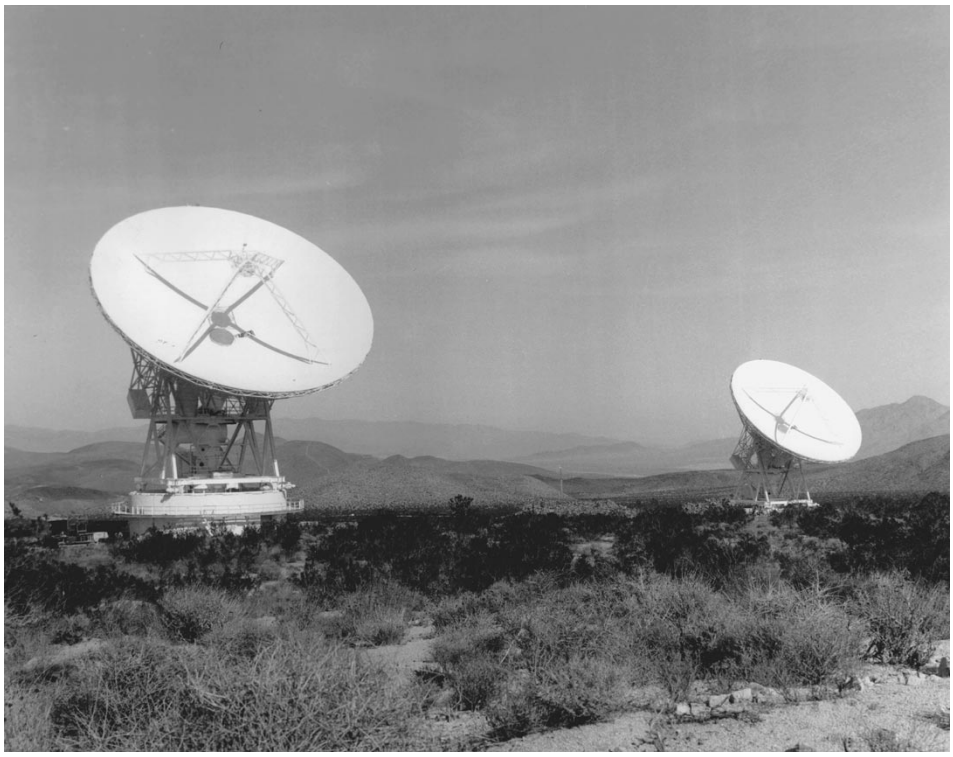

Fig. 1. Experiment site.

II. Phase-Error Budget and Measurements

In designing the prototype system, sources of error in forming a coherent signal at a target were analyzed to generate requirements for those elements of the system that could be controlled. Based upon economic considerations for the hardware and the likely variances due to nature, the phase coherence requirement was selected to be less than 11° root mean square (rms) total phase error. The RF power combining efficiency for a large number $(N > 10)$ of transmitting antennas as a function of the rms phase error among the antennas is shown in Fig. 2. The combining efficiency for only a pair of antennas is also shown in the figure for the actual phase difference between the two. The pointing loss for a 34-m-diameter antenna at 7.19 GHz is also shown in the figure. Table I shows the initial system phase error allocations.

The system performance will be affected by phase perturbations due to:

- phase control and measurement errors resulting from the hardware implementation;
- antenna structure deflections due to wind, gravity, servo system noise, temperature, and sunlight;
- transmitter phase variations due to power supply regulation and drive stability;
- phase modulation due to aspect-angle changes by the object;
- propagation path errors induced by changes in water vapor distribution and turbulence in the troposphere and ionosphere.

The system phase-path measurements must encompass as much of the actual transmitter path as possible. The transmitter and its phase delay must be included in the overall phase measurement. The delay through active microwave devices is a function of their supply voltage, for example.

A. Phase Measurement and Control Errors

Measurement errors were dominated by errors associated with signal strength. (A one-degree measurement accuracy requires a signal-to-noise ratio (SNR) of over 32 dB.) The system was implemented with transmitters having peak output power of approximately 5 kW, so SNR at acquisition was frequently on the order of 13 dB, resulting in large initial phase errors. The phase errors decreased as the target's range decreased. Object 900, LCS-1, the Lincoln Labs Calibration Sphere referenced in Barton [11], was tracked to gain data on the system phase performance at low SNR's. The average return around the point of closest approach had an SNR of 23 dB and had a mean phase error of 9.8°. The rms phase error was about 2.4 times the theoretical lower limit; however, the rms phase error met the system requirement of 11°. While receiver linearity, dynamic range, and detector effects such as in-phase/quadrature mixer gain balance and dc offsets, along with quantization effects in the digitizer are critical, careful design and implementation reduced these errors to less than 2°.

The estimated phase jitter is less than 1° rms because the master oscillator used a Hewlett Packard 8671B synthesizer. The phase reference is transmitted over a fiber-optic distribution system, which is isolated against thermal variations either by being in an air-conditioned pedestal or buried underground. A 16-bit NCO was used to set the transmitter phase resulting in a phase resolution of 0.005°.

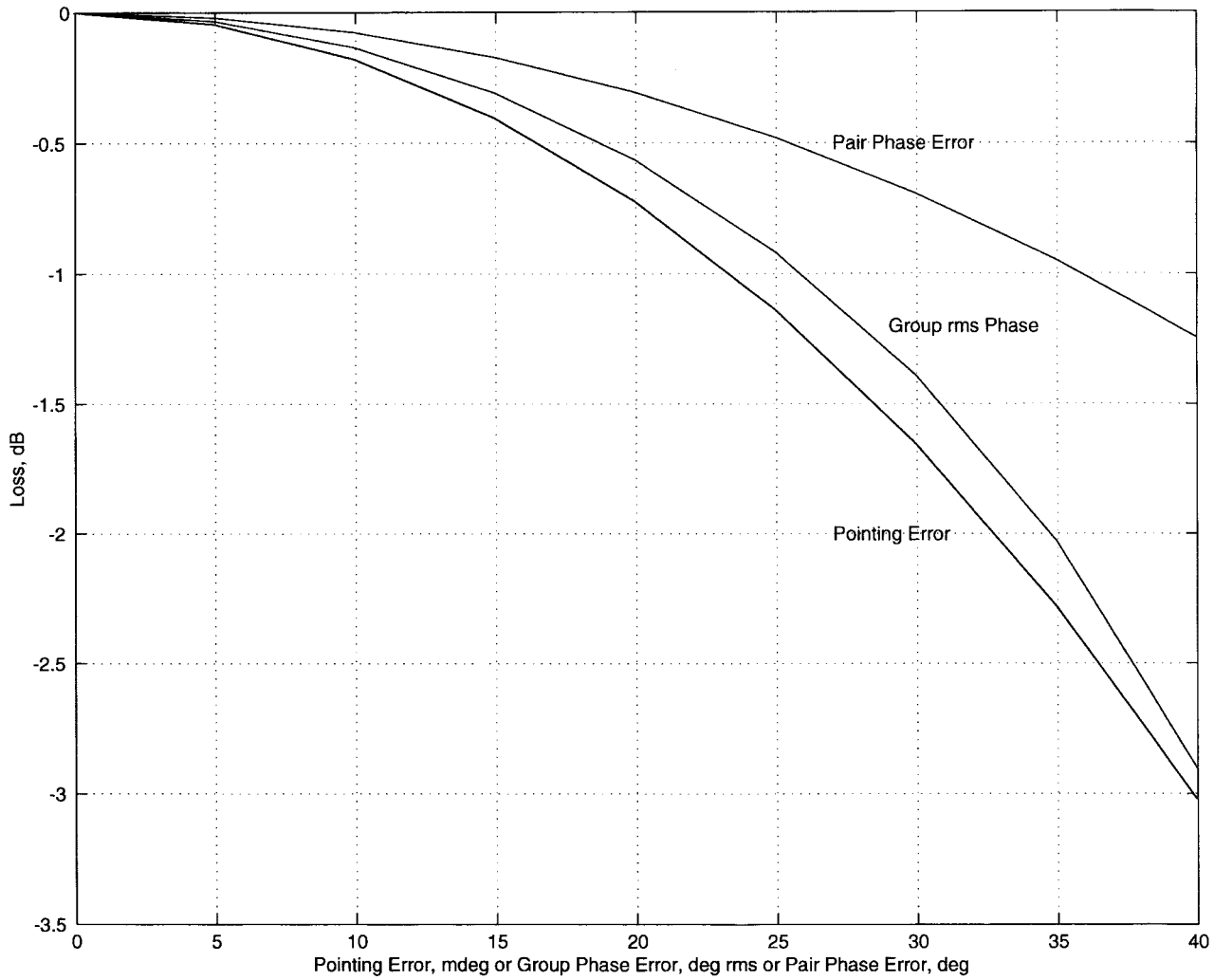

Fig. 2. System combining loss major parameters.

TABLE I
PHASING DESIGN CONTROL TABLE

Phase Error Contributor	deg
Phase control and measurement errors	
Phase Measurement error (32 dB SNR)	1.0
Computational Roundoff & Latency	0.1
Phase Reference Distribution SNR	2.0
Phase Modulator Linearity & Quantization	2.0
Structure-motion induced phase errors	
Feed Horn & BWG Mechanical and Thermal Changes	2.0
Mirror Contribution	3.0
Reflector, Quadripod & Subreflector changes due to Gravity, Wind, and Temperature	5.0
Transmitter-induced phase error	
Modulator Regulation & Transmitter Tube Pushing	2.0
Exciter Stability & Transmitter Tube AM-PM Conversion	0.4
Transmitter Tube Thermal Changes	0.6
Transmitter Tube Focus Field Stability	0.1
Waveguide Component Thermal Stability	5.0
Target-induced phase error	0.2
Troposphere & Ionosphere Residuals	7.0
RSS TOTAL	**11.2**

B. Transmitter-Induced Phase Errors

Phase changes during a transmitter pulse were found to be about $1^\circ/\mu$s of pulse width. The phase changes result from imperfect regulation of the modulator pulse voltage. This voltage is applied to the accelerator electrodes of the RF tube. Variations of the accelerating voltage lead to time-of-flight variations in the electrons in the beam that result in phase-delay variations in the tube RF output. Because the phase change was nearly linear, the transmit frequency was offset relative to the local oscillator frequency to compensate for the linear portion of the effect. Although this problem was specific to the transmitters used, similar problems will exist in almost any implementation, thus the need to calibrate the entire RF path from the RF drive signal to the transmitter through the receiver's output is manifest.

C. Structure-Motion Phase Errors

The antenna structure consisted of a 34-m-diameter reflector with a 2.5-m-diameter subreflector supported by a quadripod (four-legged) structure. An elevation-over-azimuth drive was used to point the antenna. The drive mechanism and antenna were located on a reinforced concrete structure approximately 4.5 m high and 18.3 m in diameter. Relative motions of portions of the antenna can induce phase modulation in the uplink signal. A likely candidate is the twisting of the quadripod during structural oscillations which shortens the path length between reflecting surfaces. The lowest structural resonant fre-

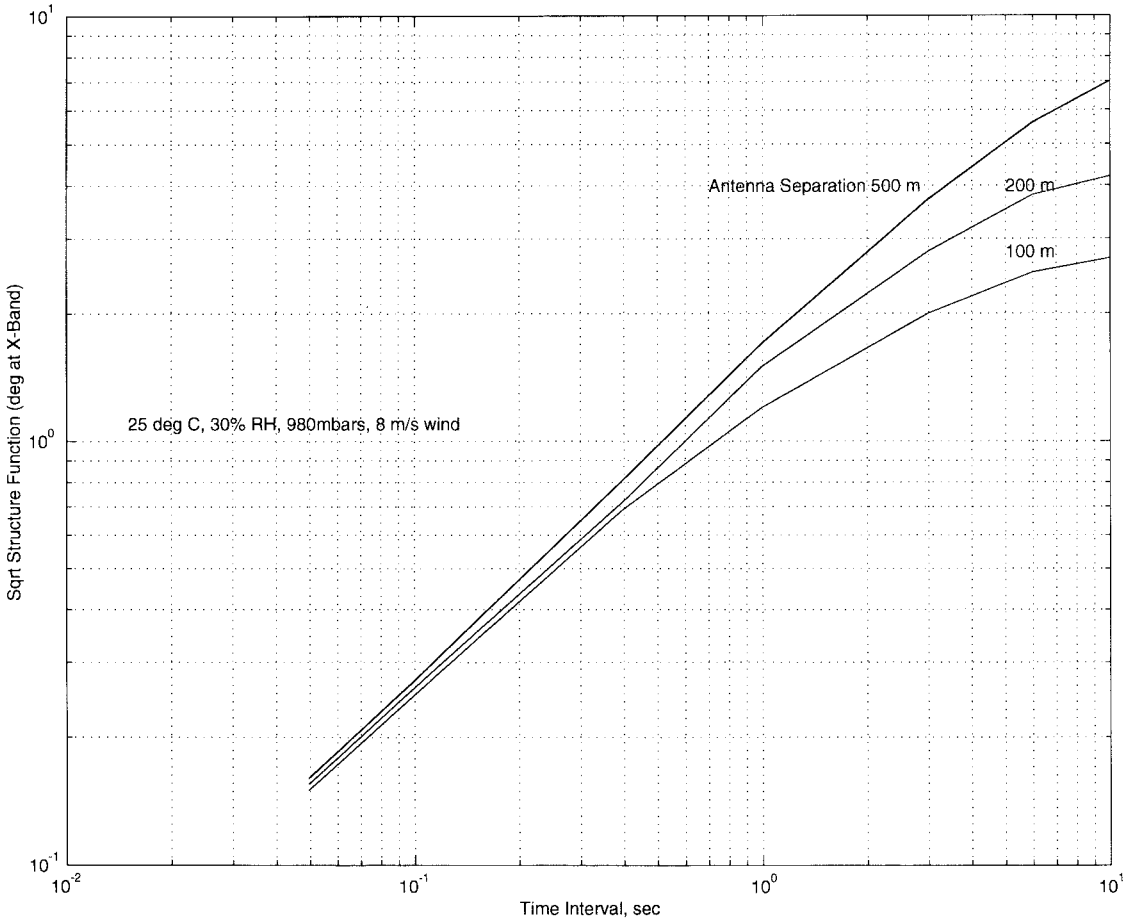

Fig. 3. Phase variation versus time for different antenna separations.

quency of the antennas used in this experiment is about 2 Hz. The calculated sensitivity of z-axis subreflector movement is 13°/mm with peak-to-peak deflections expected roughly ± 1 mm.

The phase errors due to wind-gust-excited structural resonant frequencies are measured to be less than 10° peak to peak. The phase measurements were made by comparing the transmitter output phase with the phase of a signal measured by a probe on the surface of the reflector as the antenna was excited structurally by rapid accelerations and decelerations of the drive system. These errors appear to be as significant as those caused by the tropospheric propagation path.

D. Target-Induced Phase Errors

The rotation of an elongated radar target such as a long cylinder or flat plate can cause a 180° phase reversal as the peaks of the reflected radar signal sweep past the radar receiver. In the worst case, the angle between phase reversal is equal to the wavelength of the radar divided by twice the longest dimension of the object. For example, an object 10-m long can have a phase reversal occur in 0.12° of rotation with respect to the line of sight to the radar. In an radar cross section (RCS) pattern, the two-way lobe width is one half as wide as the standard pattern of a normal antenna pattern. For example, if it were desired to have less than a 1° phase change in 1 ms, the object angular rotation rate would have to be less than 0.66°/s or one rotation per 9 min. This was not found to be a problem in the experiment since there were only two array elements making the interval between phase path-length difference measurements short compared to any significant phase changes. While the increase in system phase error due to complex shaped objects is not large enough to seriously affect the system performance, the overloading of the receive chain due to saturation of the return from a large target may have increased the measured phase errors and thus affect the phase-locked loop (PLL) performance for a few pulses.

E. Propagation-Path Phase Errors

The phase error magnitude is a function of the relative humidity (RH) and the wind relative velocity across the apertures of the antennas. A measure of the expected phase variations due to refractivity gradients resulting from troposphere turbulence is provided by the data modeled by frozen-flow wet-troposphere studies taken from the VLBI and from related interferometry activities of the DSN [3]. The NASA Propagation Handbook [12] provides similar models. Fig. 3 shows the expected phase variation across three separation distances of two antennas at Goldstone for X-band frequency as a function of time. The curves are computed for Goldstone standard daytime conditions of 25 °C temperature, 30% relative humidity, 980 millibar pressure, and average wind velocity of 8 m/s. For an interval on the order of 1 s, the

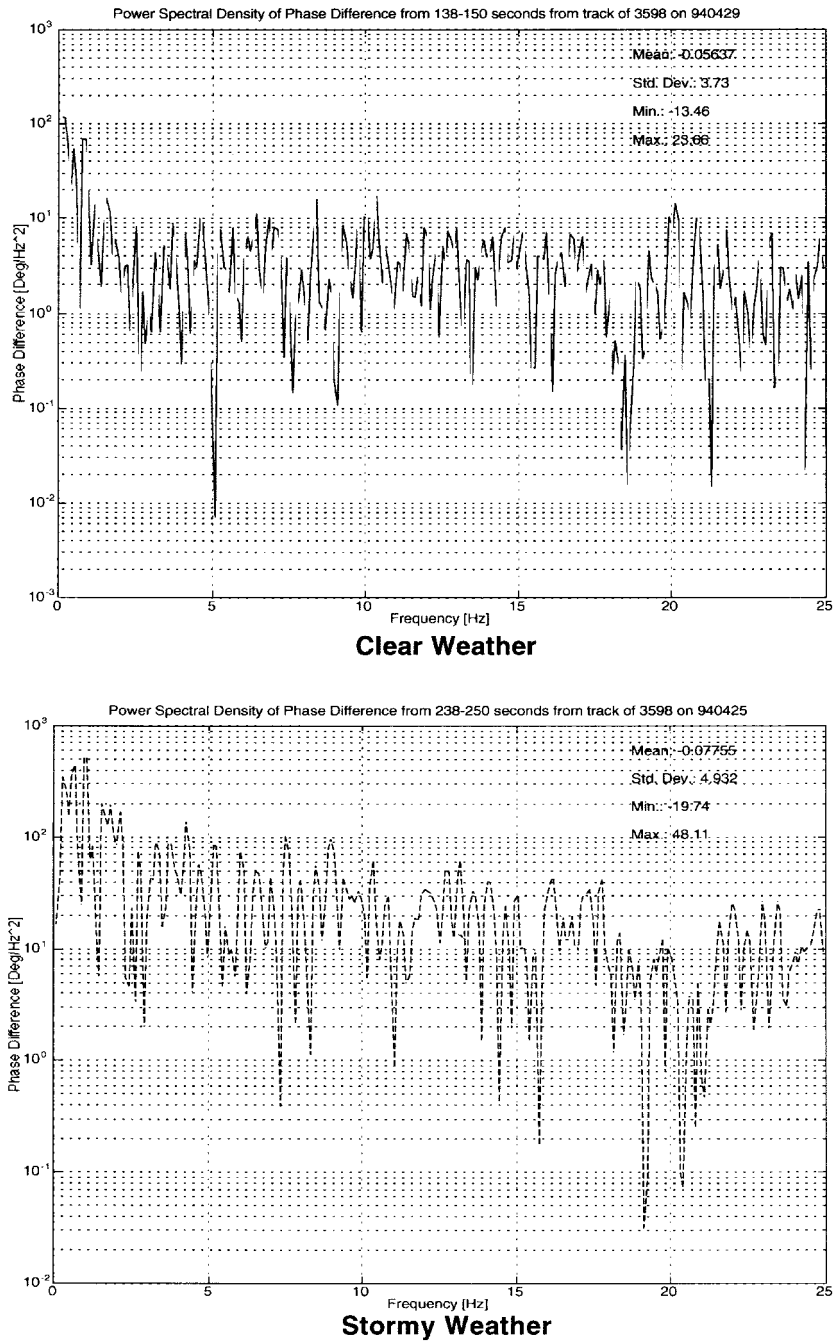

Fig. 4. Phase variance in clear and stormy weather.

phase change can be several tenths of a degree; at 10 s, it can be several degrees. The maximum expected phase difference rms magnitude for two antennas separated by 204 m is about 7°. The latter is of consequence for a system design that allows only 11° rms error. The plot is for stationary antennas and turbulence moving with a nominal wind speed of 7–8 m/s. If the beam following the object were moving through the turbulence at some higher rate, then greater phase changes are possible. Also, greater phase changes result from a higher humidity and faster wind speed.

The ionosphere has structure with waves and turbulence that can also lead to phase errors if the beams from the various antennas traverse different portions of the ionosphere. Generally, this is not expected to be a large contributor unless the array elements are very widely spaced.

Clouds were also expected to have an effect on the system performance. The phase error is a function of the cloud moisture distribution and intensity and the variation between sites. S. Slobin[1] has modeled phase changes due to clouds for tracking orbital debris at 193 km. In his worst-case model for a 1 $\mathrm{g/m^3}$ cloud with a base height of 3 km and tops at 6 km drifting over one 34-m-diameter antenna but not the other (cloud to clear or equivalent), elevation rates of 0.245°/s at 15° elevation could lead to 144°/s change at 7.145 GHz.

[1] Private communication.

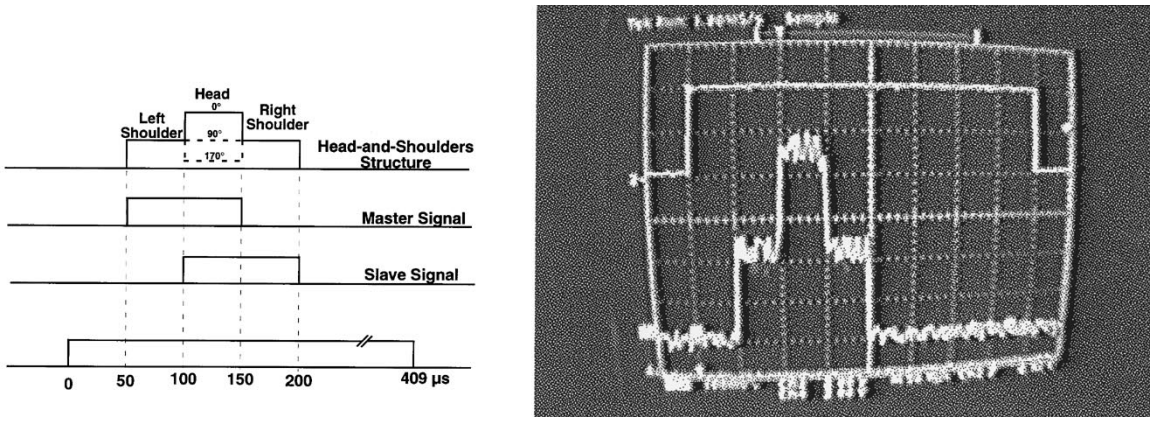

Fig. 5. Theoretical and actual received pulse structures.

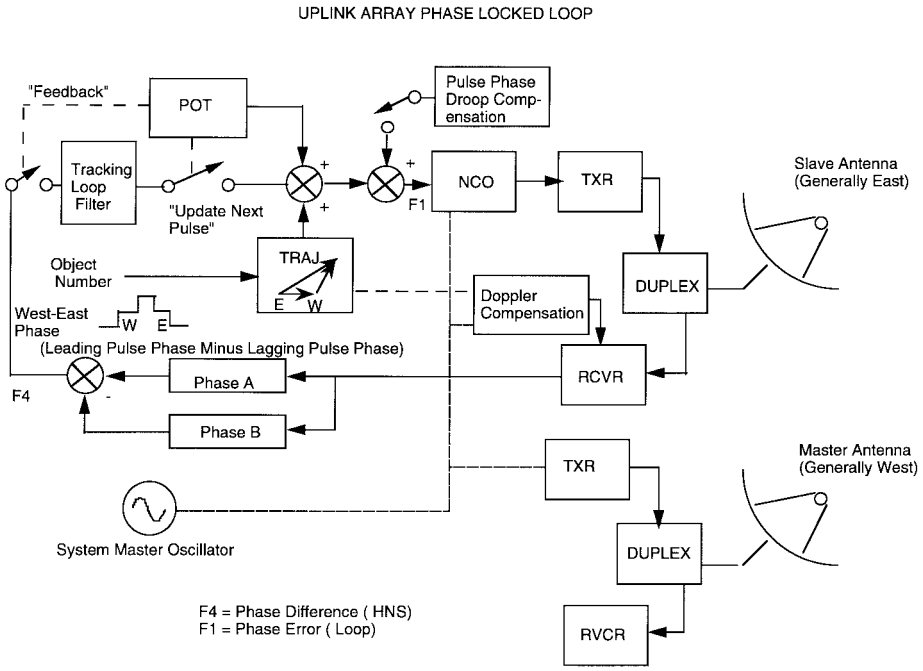

Fig. 6. Phase-locked loop.

Phase changes of less than 55°/s for that cloud model occur at elevation angles greater than 45°. For a less intense cloud model of base height 2 km and top at 4 km, the predicted phase changes were less than 50°/s at elevation angles greater than 30°.

Fig. 4 shows phase errors for tracks of the same object with and without heavy clouds. In fact, hail was reported in the vicinity of the two antennas during the recording of the data under heavy clouds conditions. The system was able to successfully maintain track under those conditions.

III. Phasing Control Design

Targets were acquired by using current orbital elements supplied by the Goddard Space Flight Center. The orbital elements' epochs were generally within a few days of the actual track, thus errors in the orbital elements were largely along-track errors which were easily compensated by adjusting the epoch by the difference between the predicted and actual time of detection. Once both antennas had started tracking the target (generally using monopulse feedback to the servo control system), the phasing experiment was started. One of the antennas was designated as the *master*. The master's phase was set to the system phase reference and never changed. The other antenna was designated as the *slave*. The receiver and phase control software in this antenna adjusted its transmitted phase so that the signal at the target was coherent.

Each transmitter normally transmitted a 100 μs pulse with about 5-kW-peak output power and a pulse-repetition frequency of 50 pulses per second. During phasing experiments, the master and slave pulses were typically offset by 50 μs to form a pulse 150 μs in length with the first 50 μs being from the master, the middle 50 μs being from the combination of slave and master and the final 50 μs being from the slave. The theoretical waveform, called "head and shoulders" is shown in Fig. 5 along with an actual received signal when the two pulses were in phase on a target.

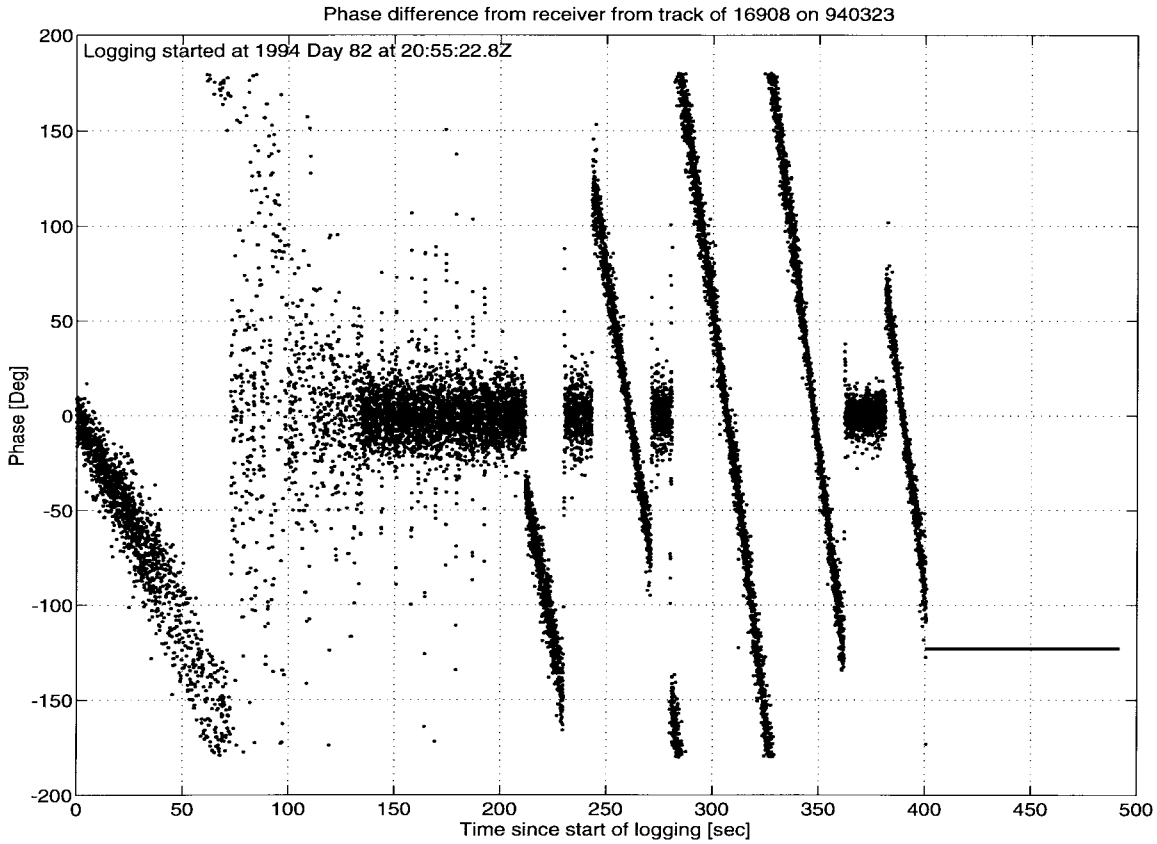

Fig. 7. Object 16 908 on 940 323, phase difference versus time.

Phase-difference measurements are made by sampling multiple times within a pulse, averaging the phase relative to the station master oscillator and then calculating the difference between the two antennas' relative phases. The phase-measuring system is provided with data samples of the return pulse digitized at 10 megasamples per second. For the complex waveform of the head-and-shoulders pulse, the leading edge 10%, the shoulder-to-head and vice versa transitional 10% and the trailing edge 10% of the data are ignored to avoid transition transients. Then depending upon the low-pass filter (LPF) in the digitizer, a variable number of samples of in-phase and quadrature are summed and averaged to yield an arctan measurement of phase relative to the station reference oscillator. For the 2500-kHz LPF, 25 samples are added, for 250 kHz (the most often utilized case), 20 samples are added, and for 25 kHz, ten samples are added.

The principal elements of the system PLL are shown in Fig. 6. A master oscillator is used to drive the master antenna transmitter and the numerically controlled oscillator (NCO) of the slave transmitter. Doppler compensation is applied only to the single, common receiver local oscillator (LO). The error in the phase-difference measurements of the two returned signals is minimized by using a common oscillator and common Doppler compensation and making phase measurements with a common receiver. The phase tracking loop is configurable as a type I, II, or III PLL, with selectable alpha, beta, and gamma parameters [13]. A pulse operation table (POT) was developed to deterministically control pulse separation, pulse width, transmit trigger, receiver data inputs to the phase loop, application of the output of the phase loop to the phase of the next pulse, as well as purposely offsetting both the timing and phase by predetermined values.

IV. System Performance

Under high SNR (>40 dB), low wind (<3.5 m/s average), low humidity, near midday conditions (with the traveling-wave tube amplifier (TWTA) operating properly) and for a nonscintillating target, the system peak-to-peak phase errors between the two antennas' received signals measured at the input to the PLL tracking loop filter, were on the order of $\pm 3°$. The rms error is estimated to be less than 1°. The theoretical peak-to-peak phase measurement error for a 40-dB SNR signal limited by thermal noise is 0.57°.

A calibration sphere—object 5398—was tracked under benign conditions with very low wind speed (0.04 m/s average) and with low humidity (27%). The peak SNR for a shoulder was 27 dB. The peak wind speed was less than 1.3 m/s during the track. The digitizer was calibrated as part of the normal system initialization. The rms phase error was 4.4°, which is slightly higher than the thermal limit of 2.5°.

Some experiments were conducted where the phase loop was opened during the track to determine the system behavior once a static phase calibration had been completed. Fig. 7 shows the phase error during such an experiment. The object tracked is a spherical optical target which carries 318 flat mirrors (approximately 20 $\times$ 20 cm) interspersed with 120 laser reflectors (1436 corner cubes) and represents an extreme

case of a scintillating target. The phase error starts to increase linearly as soon as the phase loop is opened (at 210, 245, 270, and 390 s from the start of logging). In each case, the phase error increased linearly. Subsequent analysis concluded that the phase error increase was caused by a systematic error in the initial orbit correction which resulted in an error in the path-length difference between the two radars. Phase errors caused by atmospheric disturbances would not have been so linear.

The linear change in phase error was observed on several other tracks; unfortunately, the experiment was terminated before the source of the error could be confirmed as being due to errors in the orbital element update technique. Regardless of the source of error, even if it cannot be eliminated, the error is predictable and can be corrected. The phase errors were also insensitive to the angular tracking range; therefore, it is likely that a calibration could first be made using exo-atmospheric debris followed by moving the antennas by a few degrees to point to the desired location without adversely affecting the calibration.

V. Conclusion

Based on the experiments performed, it is feasible to construct a high-power radar or communication uplink from a set of relatively small and inexpensive transmitting elements. System phase adjustments can be made periodically on signals returned from orbital debris to remove tropospheric, ionospheric, and equipment phase variations. Uplink arraying of the transmitting antennas that move at side real rates should be possible for perhaps hours at a time once a system calibration has been effected for the static phase errors. Factors that significantly reduce that time are:

- adverse weather, such as thick clouds (greater than 2 km thick at 1 g/m^3), rain, high winds (greater than 22 m/s), or rapid temperature changes (greater than 20 °C per hour and 10% of the phase change as differential between sites);
- phase instability in the transmitting equipment.

Any significant phase errors due to tropospheric inhomogeneities were not observed but may have been present at a reduced magnitude. Antenna structure deflections were observed to cause phase errors equal to troposphere effects, but only under significant accelerations. Target-induced phase errors (e.g., scintillation) were not found to induce significant phase errors over the short period required for a phase calibration. The "head and shoulders" waveform proved to be convenient for observing phasing performance.

References

[1] R. K. Crane, "Fundamental limitations caused by RF propagation," in *Proc. IEEE*, vol. 69, pp. 196–209, Feb. 1981.
[2] S. D. Slobin, "Microwave noise temperature and attenuation of clouds: Statistics of these effects at various sites in the United States, Alaska, and Hawaii," *Radio Sci.*, vol. 17, pp. 1443–1454, Nov./Dec. 1982.
[3] Treuhaft and G. E. Lanyi, "The effect of the dynamic wet troposphere on radio interferometric measurements," *Radio Sci.*, vol. 22, pp. 251–265, 1978.
[4] A. D. Goldfinger, "Refraction of microwave signals by water vapor," *J. Geophys. Res.*, vol. 85, no. C9, pp. 4904–4912, Sept. 1980.
[5] M. C. Thompson, F. E. Marler, and K. C. Allen, "Measurement of the microwave structure constant profile," *IEEE Trans. Antennas Propagat.*, vol. AP-28, pp. 278–280, Mar. 1980.
[6] T. E. VanZandt, J. L. Green, K. S. Gage, and W. L. Clark, "Vertical profiles of refractivity turbulence structure constant: Comparison of observations by the sunset radar with a new theoretical model," *Radio Sci.*, vol. 13, no. 5, pp. 819–829, Sept./Oct. 1978.
[7] H. Ottersten, "Atmospheric structure and radar backscattering in clear air," *Radio Sci.*, vol. 4, no. 12, pp. 1179–1193, Dec. 1969.
[8] J. W. Eberle, "An adaptively phased, four-element array of thirty-foot parabolic reflectors for passive (echo) communication systems," *IEEE Trans. Antennas Propagat.*, vol. AP-12, pp. 169–176, Mar. 1964.
[9] J. K. Dempsey, W. Mullins, R. D. Barber, D. L. Losh, A. M. Bhanjo, and R. M. Dickinson, "A high-power phased array transmitter facility," in *Proc. 7th Nat. Conf. High-Power Microwave Technol.*, Naval Postgraduate School, Monterey, CA, Oct. 31–Nov. 4, 1994.
[10] G. J. Friedman, "Risk management applied to planetary defense," *IEEE Trans. Aerosp. Electron. Syst.*, vol. 33, pp. 721–733, Apr. 1997.
[11] D. K. Barton, *Modern Radar System Analysis*. Norwood, MA: Artech House, 1988.
[12] W. L. Flock, "Propagation effects on satellites systems at frequencies below 10 GHz," NASA Ref. Publ. 1108, Washington, DC, 1983.
[13] P. A. Kalata, "The tracking index: A generalized parameter for a-b and a-b-g target trackers," *IEEE Trans. Aerosp. Electron. Syst.*, vol. AES-20, pp. 174–182, Mar. 1984.

Richard M. Dickinson (S'56–M'58–SM'83–LS'97) received the B.S.E.E. degree from Auburn University, Auburn, AL, in 1958, and the M.S.E.E. degree from the University of Texas-Austin in 1962.

He is currently a Multidisciplinary Senior Engineer at the Jet Propulsion Laboratory (JPL), California Institute of Technology, Pasadena. As a Microwave Power Systems Engineer in the Communications Ground Systems Section of the Telecommunications Science and Engineering Division, he is currently involved in studying and designing the solar-pumped laser-power beaming phased array for interstellar missions. In his 35 years at JPL, he has developed high-power transmitters and antennas for both Mariner and Voyager spacecraft and ground stations of the NASA Deep Space Network. The first X-band transmitter on the Mariner-Venus 1973 spacecraft for use in S/X-Band dispersive charged particle experiments was developed in the Spacecraft Transmitter Development Group, which he supervised. He also supervised the ground-based 500-kW CW S and X-Band Transmitter Development Group. He investigated the technology for the microwave power transmission link of the NASA-DOE proposed Satellite Power System (SPS) as the wireless power transmission specialist on the NASA study team. In a test with Raytheon in 1975, he, along with others, demonstrated an end-to-end (dc to dc) power transfer efficiency of over 54% using 2.45 GHz microwaves. He was Project Manager of a demonstration of transmitting microwave power at 2.388 GHz and recovering over 34 kW of dc power at a range of 1.6 km at Goldstone, CA in 1975. He spent nine months at the Japanese Institute of Space and Astronautical Sciences in 1988 as a detailee from JPL providing liaison for the Voyager Neptune encounter. He also worked in the JPL International Affairs Office in the Far East Desk. He participated in the NASA Fresh Look Space Solar Power Study and delivered a paper to the International Telecommunications Study Groups on "information leading to a draft new recommendation regarding wireless power transmission" at Geneva, Switzerland, in July 1997. His prior studies have involved foliated terrain propagation, Mars Rover comm links and comparison of X band, Ka band, and optical links for deep-space communication. He was Systems Engineer of the design and operation of a successful uplink arraying radar experiment using two 34-m-diameter antennas at X band in 1994 and Systems Engineer for a study of beamed power to a circling aircraft for telecommunications and observations platform. He has consulted for Universal Studios, JFD Electronics, LTI Robotics Systems, A.D. Little, SRI International, and Maxwell Laboratories. He has four patents in the Microwave field

Mr. Dickinson has been a member of the NASA Communications Technology Working Group, was chairman of the Communications Working Group of the Space Station Technology Steering Committee. He was coeditor of the June 1992 IEEE Microwave Theory and Technique Special Issue on Microwaves in Space. He is a member of Sigma XI

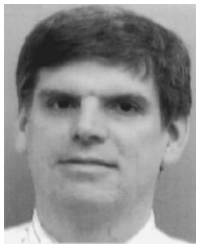

David L. Losh received the B.S. degree in physics from Case Institute of Technology, Cleveland, OH, in 1970, and the M.S. degree in computer science from University of Southern California, Los Angeles, in 1980.

In his position as a Senior Telecommunications Engineer in the Communications Ground Systems Section, he is the Cognizant Development Engineer for a pair of 20-kW transmitters that will be installed on the 70-m antennas of the deep-space network to support the Cassini mission to Saturn. Previous work at the Jet Propulsion Laboratory, Pasadena, CA, includes Task Manager for a microwave-powered aircraft to provide telecommunications services to sparsely populated areas. He has performed systems engineering and integration and has served as the Experiment Director of the system described in this paper.

Robert Dan Barber received the B.S.A.E. degree from Auburn University, Auburn, AL, in 1966.

He began his professional career with Douglas Aircraft, Huntington Beach, CA, working as an Engineer/Scientist on the SATURN S-IVB Program. He began his federal government career in 1971 and for most of the time since then has worked for the U.S. Army in the field of directed energy. He has worked in testing and data analysis, investigating advanced concepts in the fields of laser and RF energy. He has also directed research in both technical areas and is currently Chief of the Unconventional Beam Office, Weapons Sciences Directorate, U.S. Army Aviation and Missile Command, Rodstone Arsenal, AL.

John K. Dempsey received the B.S.E.E. degree from the University of Alabama, Huntsville, in 1982.

He has held a research position as an Electronics Engineer with the U.S. Army Aviation and Missile Command (USAAMCOM), Rodstone Arsenal, AL, since that time. He has served in various capacities within the field of directed energy, both as a team member and in lead roles. He has been involved in several successful programs involving the research, development, and testing of laser and RF technologies for army applications including the antenna research system described in this paper. He is currently working for the U.S. Army Space and Missile Defense Command (USASMDC), Huntsville, AL.